# Study on fabrication of grinding wheel in Selective Laser Melting

Li Shuai[1, 2, a], Zhang Bi[2, b, *], Zhou Cong[2, c]

[1] School of Mechatronics Engineering, Harbin Institute of Technology, Harbin, 150001, China

[2] Department of Mechanical and Energy Engineering, Southern University of Science and Technology, Shenzhen, 518055, China

[a]11849534@mail.sustech.edu.cn, [b] zhangb@sustech.edu.cn, [c] zhouc@sustech.edu.cn

**Keywords:** Selective laser melting (SLM), grinding wheels, single track, chemical distribution

**Abstract.** Selective laser melting (SLM) is a promising technique to build grinding wheels with complex structures. In this paper, Ni-based self-fluxing alloys are chosen as bond materials to investigate single track formation on a steel substrate under different processing parameters. Results show that irregular and balling tracks are obtained with a low linear energy density (LED). The width of a melt pool increases linearly with LED. For LED values larger than around 0.9 J/mm, keyhole occurs in the melt pool, which is not desirable in the SLM process. Energy dispersive spectroscopy (EDS) mapping is performed to investigate the formation of the melt pool. Through an analysis on chemical distributions, it is found that the melt pool has a mixture of the partly melted substrate and powders. However, in the keyhole region, only the alloying elements of the substrate are detected due to the repulsion of the melted powder materials caused by the recoil pressure. This work can offer guidance on parameter optimization for the fabrication of SLMed grinding wheels.

## 1. Introduction

As an additive manufacturing technique, Selective Laser Melting (SLM) has widely been applied to many industries, including medicine, electronic, automotive, and aerospace. Based on powder melting layer by layer at 20-100 μm, SLM possesses promising capabilities of producing parts with complex geometries, such as porous or lattice lightweight structures [1-3]. The mechanical properties of an SLMed metallic part can be comparable to its wrought counterpart. Also, functionally graded multi-material parts and particle reinforced composites can be fabricated by SLM [4]. However, defects in the as-built parts such as porosities, balling, cracks, and rough surface, are detrimental to the final mechanical properties of SLMed part [5]. Many researches have been carried out to reduce or eliminate the defects in SLMed parts. However, these defects have little effect on the properties of a grinding wheel. Porosities in the grinding wheel play a significant role in a grinding process. High porosities in a grinding wheel can provide enough space to accommodate grinding fluid and debris, leading to a lower grinding temperature rise and less clogging [6]. Cracks can enhance the self-sharpening ability of a metal-bonded grinding wheel.

A metal-bond grinding wheel is normally manufactured through hot-press sintering (HPS), electroplating, or brazing. However, HPS can hardly fabricate grinding wheels with a high porosity ratio and complex structures [7]. For electroplating and brazing grinding wheels, the thickness of the abrasive layer is greatly limited, reducing the life of the grinding wheels. Combined with the advantages of additive manufacturing, grinding wheels with a complex structure and high porosity ratio can be fabricated. In addition, the arrangement of abrasives and porosities can be controlled.

Studies have been carried out to fabricate grinding wheels by additive manufacturing. Spierings et al. [8] took a feasibility study on fabrication of grinding wheels with the Cu-Sn-Ti brazing alloys in SLM. Metal-diamond composites with 10 Vol% and 20 Vol% Ni-coated diamonds were fabricated, within which a few cracks and little graphitization of diamond occurred. Yang et al. [9] applied a CNC laser machine to fabricate grinding wheels with a regular grain distribution. The arrangement of diamond grains could be controlled by a feeding device. Qiu et al. [10] developed a stereolithography apparatus to produce a resin-bonded grinding wheel with the optimized diamond arrangement. Through additive manufacturing, the internal structure and porosities could be fabricated and controlled. Du et al. [11] used selective laser sintering to fabricate grinding wheels

with internal cooling holes to improve grinding performance. Tian et al. [3, 6, 12] fabricated SLMed grinding wheels with controllable porosity shapes, sizes, and distributions through the designed cellular structures. The porosity ratio of the grinding wheel was maintained at 53% or higher, offering good cooling and lubrication conditions.

Due to the track-by-track process, the quality of an SLMed part often shows its quality greatly influenced by the individual tracks. Investigation on the formation process of the individual tracks is beneficial to understanding physical phenomena such as heat transfer, fluid flow, and mass transfer in a melt pool. In addition, processing parameters can be optimized through an analysis on melt pool dimensions [13, 14]. In this paper, single tracks of the Ni-based alloys are formed on a steel substrate at different laser power levels and scanning speeds. The quality of the single tracks and melt pool dimensions are analyzed for parameter optimization in fabrication of SLMed grinding wheels. Mass transfer of a melt pool in both conduction mode and keyhole mode is studied through energy dispersive spectroscopy (EDS) mapping.

## 2. Experimental procedures

### *2.1 Materials and experimental conditions*

The NiCrBSi self-fluxing alloy was chosen as a bind material that has a melting point 970-1000 °C. The substrate was made by the AISI 1045 steel. Chemical compositions of the powder and substrate are given in Table 1. Based on the previous studies on NiCrBSi [9], Cr could enhance the wettability of the bind material to diamond abrasives, B and Si were effective in lowering the melting point. The gas-atomized powders with spherical shape were used in the experiment. The powders have the particle size distribution shown in Fig. 1.

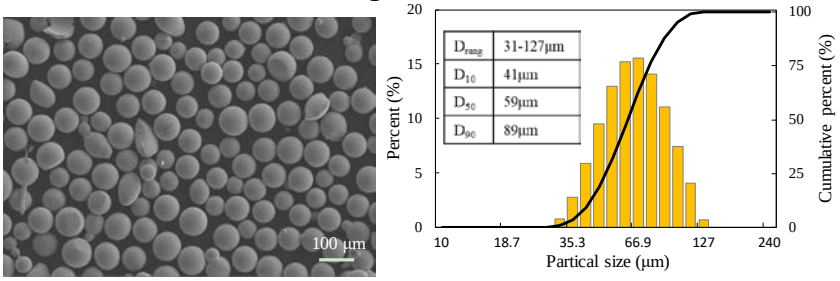


(a) (b)

**Figure 1.** (a) SEM images of the NiCrBSi powder, (b) particle size range

**Table 1.** Chemical compositions of the powder and substrate (wt.%)

| Chemical compositions (wt.%) | | | | | | | |
|---|---|---|---|---|---|---|---|
| | Ni | Cr | Fe | B | Si | C | Mn |
| **Powder** | Bal | 7.0 | 3.0 | 3.1 | 4.5 | | |
| **Substrate** | | ≤0.25 | Bal | | | 0.42-0.50 | 0.5-0.8 |

**Table 2.** Processing parameters for single track in SLM

| Parameters | Values |
|---|---|
| Laser spot size, *D* | 120 μm |
| Powder layer thickness, *h* | 100 μm |
| Laser power, *P* | 80,100,120,140, 160, 200, 240 W |
| Scanning speed, *V* | 100, 150, 200, 250 mm/s |

SLM equipment (Dimetal-100H, Guangzhou Laseradd Technology Corporation) with a maximum laser power 250 W was used in the experiment. A defocusing Gaussian laser beam was applied to gaining a large spot. The defocus distance was 2 mm and diameter of the laser spot (*D*) was about 120 μm. The thickness of the powder layer (*h*) was 100 μm. Before the experiment, sandblasting treatment was performed on the substrate. A series of single tracks were fabricated on

the substrate at various laser powers ($P$) and scanning speeds ($V$), as listed in Table 2. All the experiments took place under a protective argon atmosphere.

*2.2 Morphological characterization*

The surface morphology of single tracks was observed by the ultra-depth 3D microscopy (Keyence, NHX-7000) and confocal laser scanning microscopy (Keyence, VK-X1000). Cross-sections perpendicular to the scanning direction were prepared, polished and etched for evaluating the width ($w$), height ($h$) and depth ($d$) of the single tracks. The dimensions were measured at three different locations in continuous tracks without balling. Scanning electron microscopy (SEM, Zeiss Merlin) and energy dispersive spectroscopy (EDS) were performed to determine the element distributions.

## 3. Results and Discussion

*3.1 Track morphology*

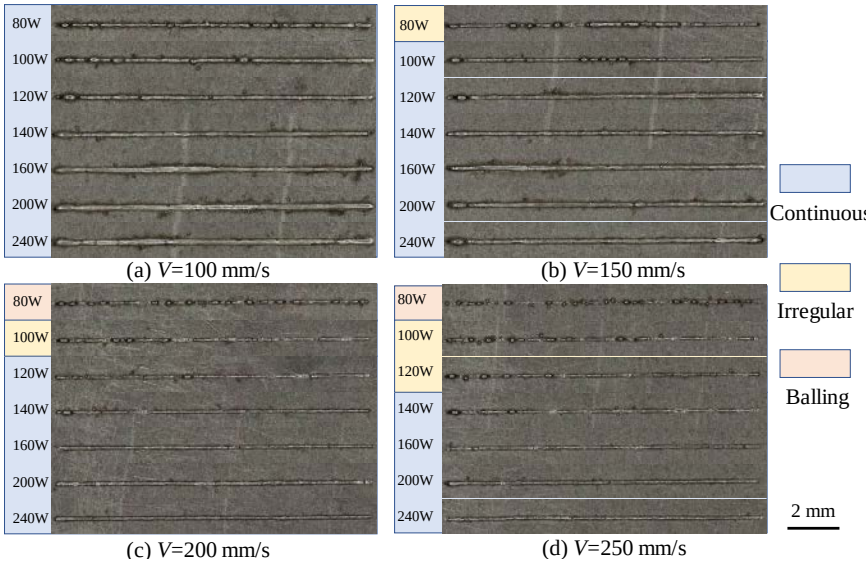


**Figure 2.** Confocal images of the single tracks of the SLM deposited NiCrBSi alloy with different parameters

The surface morphologies of single tracks under different laser powers and scanning speeds are shown in Fig. 2. Three types of track morphologies, including continuous, irregular, and balling, can be found [15]. All the tracks were continuous with a scanning speed of 100 mm/s. As the scanning speed was increased to 150 mm/s, irregular tracks were formed. Balling tracks and barely connected metal droplets occurred at a higher scanning speed of 250 mm/s. The track morphology was associated with the Linear Energy Density (LED), which is defined as LED = $P/V$. At low LED values, the substrate was barely melted and the melt pool of powders changed from the comet-like shape to the spherical beads due to the surface tension. Because of the Plateau-Rayleigh instability, a melt-free cylindrical shape tended to break up into an array of small droplets [13, 16].

Two types of melt pools were observed through the cross-sectional analysis, i.e., conduction mode and keyhole mode. The cross-sections were etched by ethanol solution of 4% $HNO_3$ for 10 seconds to distinguish the melt pool from substrate. Since the NiCrBSi alloy could hardly be etched by the etchant, the melt pool showed a bright region by the optical microscopy, as shown in Fig. 3. In the conduction mode, the mixed melt pool exhibited a shallow semicircular shape. A heat affected zone (HAZ) was formed between the melt pool and substrate. In HAZ, quenching and tempering processes occurred because the temperature was insufficient for dissolution of the material grains. In the keyhole mode, the depth of the melt pool was several times of the width. An interface divided the melt pool into two regions. The bright region was similar to the melt pool in the conduction mode, while the grey region existed in the bottom after etching. It is assumed that the bottom part hardly contains the elements from the supply powders, which was confirmed by EDS mapping. In the middle

and at the left and right sides of the interface, the mixed melt pool extended down into the grey region, showing an “M” profile.

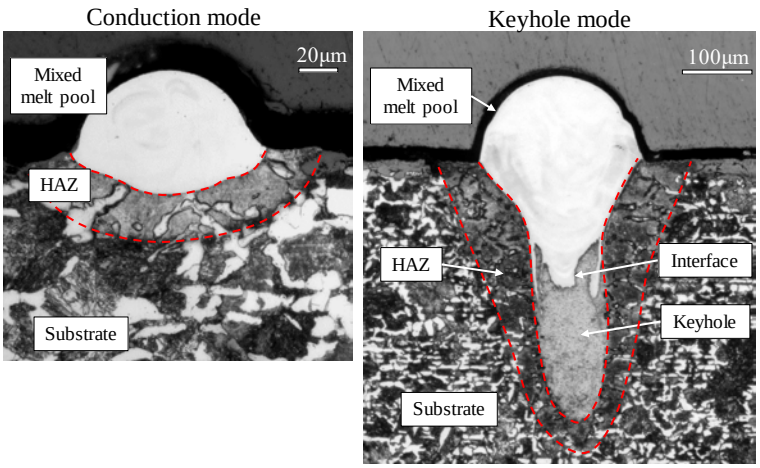


**Figure 3.** Melt pool morphology of the conduction mode (left) and the keyhole mode (right)

*3.2 Geometry measurements*

The dimensions of the melt pool are shown in Fig. 4. A roughly linear relationship between the width and LED is found. A large LED value means excess energy input, leading to an intensive heat flow to melt the nearby particles and increasing track width. Furthermore, the scanning speed does not seem to affect the track width as the LED values are identical.

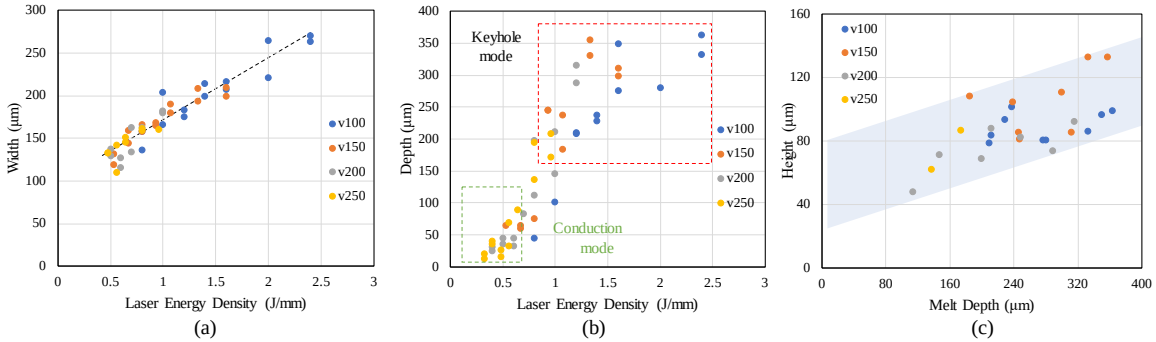


**Figure 4.** Geometry analysis of the melt pool at different parameters (a) Width; (b) Depth; (c) Height

The melt pool depths in both the conduction and keyhole modes are plotted in Fig. 4(b). An increasing trend of the track depth with LED can be observed. Conduction mode was obtained with LED lower than 0.75 J/mm. When LED was larger than 0.9 J/mm, keyhole formed in the melt pool. The shift from the conduction mode to the keyhole mode was not quite clear due to large data deviation. For example, both conduction and keyhole modes were observed with a melt depth ranging from 45 μm to 200 μm. The data scattering was caused by the unstable interaction between the laser beam and the melt pool. Also, spatters had a great effect on the melt pool depth due to laser shadowing [17]. A large melt pool depth is not desired because the previous layer may be melted, causing a high level of the thermal residual stresses.

According to a study of Yadroitsev et al. [13], the major factor of melt pool height is layer thickness. While in this paper, the height of a melt pool increases with melting depth, as shown in Fig. 4(c). Actually, the depth of a melt pool is a reflection of laser energy absorption. Nearby particles can be melted and converged into the melt pool with large laser energy absorption, leading to an increase in the melt pool height.

*3.3 Chemical distribution inside the mixed melt pool*

In general, the mixed melt pool is composed of both powder and substrate materials. Particularly in the keyhole mode, the mixed melt pool is divide into two regions, as shown in Fig. 3(b). In order to study the formation of a melt pool, chemical distributions of Fe and Ni were obtained by EDS

mapping, as shown in Fig. 5. Fe and Ni are the primary elements in the substrate and NiCrBSi powders, respectively.

Inside a melt pool of the conduction mode, the top region was concentrated with more Fe, but with less Ni. Chemical segregation occurred due to flow in the melt pool, which was driven by thermos-capillary convection, i.e., the Marangoni convection. Due to the rapid solidification in the SLM process, the melted powders and substrate were hardly well mixed.

In the keyhole mode, chemical segregation got more obvious in the mixed melt pool, as shown in Fig. 5(b)-(I). In the top region of the melt pool, the Fe element took an approximately round shape in the middle, and is surrounded by the Ni element. A swirl-like pattern was observed in the bottom region of the mixed melt pool, as shown in Fig. 5(b)-(II). The mixed melt pool extended down at the left and right sides of the interface. In the keyhole region, the elements from the supplying powders were hardly detected. The characteristics of the melt pool in keyhole mode were exactly associated with intensive laser radiation, causing metal vapor and strong fluid flow. When metal vapor occurred, recoil pressure was induced and the melted powders were pushed to the sides of the melt pool [17]. Thus melted powders could hardly get into the keyhole region. As recoil pressure decreased or vanished, the melted powders flowed toward the middle to mix with melted substrate due to Marangoni convection.

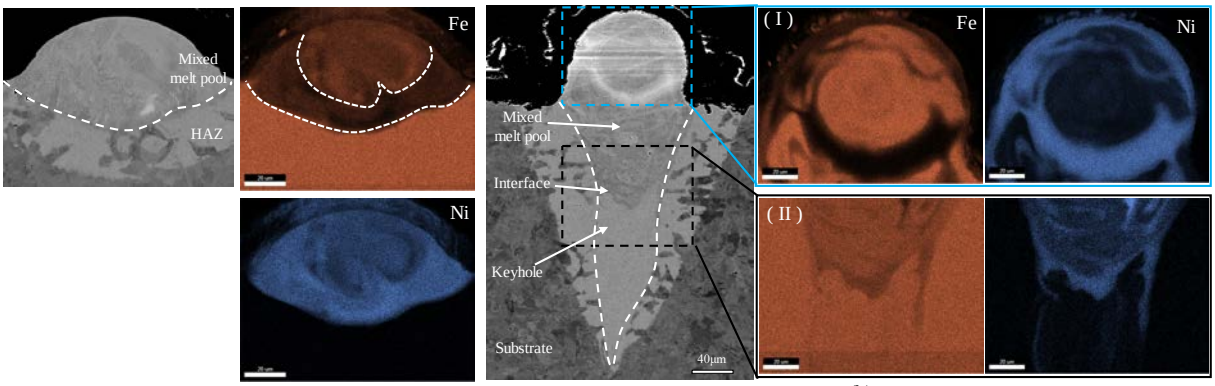


**Figure 5.** Chemical distributions in the melt pool: (a) conduction mode; (b) keyhole mode – the top region (I) and the bottom region (II) of the mixed melt pool

## 4. Conclusions

In this paper, selective laser melting was adopted to fabricate grinding wheel bond with the NiCrBSi self-fluxing alloys on a steel substrate with single tracks. The paper investigated and analyzed the morphology and dimensions of the melt pool of the SLM tracks. The element distributions were also studied to understand the melt pool formation. The following conclusions can be drawn,

- Continuous tracks are obtained with a proper LED and scanning speed. In a low LED, irregular and balling tracks are formed.
- A linear relationship of the melt pool width with LED is established. The melt pool roughly shifts from the conduction mode to the keyhole mode at an LED level larger than 0.75 J/mm. An increasing trend of track height with melting depth is observed.
- The melt pool contains a mixture of the elements from the supplying powders and substrate, which leads to element segregation. No elements from the supplying powders are detected in the keyhole region due to the recoil pressure generated by the intensive laser radiation.


## Acknowledgements

The authors gratefully acknowledge the financial support from the Shenzhen Science and Technology Innovation Commission for the projects numbered as: Y01336107, GJHZ20180411143506667, and JCYJ20170817111811303.

**References**


[1] Mazur M, Leary M, Sun S, Vcelka M, Shidid D, Brandt M. Deformation and failure behaviour of Ti-6Al-4V lattice structures manufactured by selective laser melting (SLM). *Int J Adv Manuf Tech*, 2016, 84(5-8): 1391-411.

[2] Amin Yavari S, Ahmadi SM, Wauthle R, Pouran B, Schrooten J, Weinans H, et al. Relationship between unit cell type and porosity and the fatigue behavior of selective laser melted meta-biomaterials. *J Mech Behav Biomed*, 2015, 43: 91-100.

[3] Tian C, Li X, Chen Z, Guo G, Rong Y. Study on formability, mechanical property and finite element modeling of 3D-printed composite for metal-bonded diamond grinding wheel application. *J Manuf Process*, 2020, 54: 38-47.

[4] Bartolomeu F, Buciumeanu M, Pinto E, Alves N, Carvalho O, Silva FS, et al. 316L stainless steel mechanical and tribological behavior–A comparison between selective laser melting, hot pressing and conventional casting. *Addit Manuf*, 2017: 81-9.

[5] Zhang B, Li Y, Bai Q. Defect Formation Mechanisms in Selective Laser Melting: A Review. *Chin J Mech Eng*, 2017, 30(3): 515-27.

[6] Tian C, Li X, Li H, Guo G, Wang L, Rong Y. The effect of porosity on the mechanical property of metal-bonded diamond grinding wheel fabricated by selective laser melting (SLM). *Mat Sci Eng A-Struct*, 2019, 743: 697-706.

[7] Song CJ, Ding WF, Xu JH, Chen ZZ. Grinding Performance of Metal-Bonded CBN Wheels with Regular Pores. *Appl Mech Mater*, 2012, 217-219: 1857-62.

[8] Spierings AB, Leinenbach C, Kenel C, Wegener K. Processing of metal-diamond-composites using selective laser melting. *Rapid Prototyping J*, 2014, 21(2): 130-6.

[9] Yang Z, Zhang M, Zhang Z, Liu A, Yang R, Liu S. A study on diamond grinding wheels with regular grain distribution using additive manufacturing (AM) technology. *Mater Design*, 2016, 104: 292-7.

[10] Qiu Y, Huang H. Research on the fabrication and grinding performance of 3-dimensional controllable abrasive arrangement wheels. *Int J Adv Manuf Tech*, 2019, 104(5): 1839-53.

[11] Du Z, Zhang F, Xu Q, Huang Y, Li M, Huang H, et al. Selective laser sintering and grinding performance of resin bond diamond grinding wheels with arrayed internal cooling holes. *Ceram Int*, 2019, 45(16): 20873-81.

[12] Tian CC, Li X, Shubo Z, Guo G, Rong Y. Porous structure design and fabrication of metal-bonded diamond grinding wheel based on selective laser melting (SLM). *Int J Adv Manuf Tech*, 2019, 100(5-8): 1451-62.

[13] Yadroitsev I, Gusarov AV, Yadroitsava I, Smurov I. Single track formation in selective laser melting of metal powders. *J Mater Process Tech*, 2010, 210(12): 1624-31.

[14] Yadroitsev I, Krakhmalev P, Yadroitsava I, Johansson S, Smurov I. Energy input effect on morphology and microstructure of selective laser melting single track from metallic powder. *J Mater Process Tech*, 2013, 213(4): 606-13.

[15] Bertoli US, Wolfer AJ, Matthews MJ, Delplanque JR, Schoenung JM. On the limitations of Volumetric Energy Density as a design parameter for Selective Laser Melting. *Mater Design*, 2017, 113: 331-40.

[16] Guo Y, Jia L, Kong B, Wang N, Zhang H. Single track and single layer formation in selective laser melting of niobium solid solution alloy. *Chinese J Aeronaut*, 2017, 31(4): 860-6.

[17] Khairallah SA, Martin AA, Lee JRI, Guss G, Calta NP, Hammons JA, et al. Controlling interdependent meso-nanosecond dynamics and defect generation in metal 3D printing. *Science*, 2020, 368(6491): 660-665.